C/No Assessment Based on GPS L5/L1C/A Signal Acquisition in Open-Sky/Light-Urban/Dense-Urban/Indoor Environments with Extended Coherent Integration Time

Article *in* Journal of Aeronautics, Astronautics and Aviation, Series A · January 2022

DOI: 10.6125/JoAAA.202306_55(2).06

CITATIONS
0

READS
59

4 authors:

Chin Lok Auston Tsang
The Hong Kong Polytechnic University
3 PUBLICATIONS **1** CITATION
SEE PROFILE

Yiran Luo
The University of Calgary
36 PUBLICATIONS **238** CITATIONS
SEE PROFILE

Bing Xu
The Hong Kong Polytechnic University
40 PUBLICATIONS **285** CITATIONS
SEE PROFILE

Li-Ta Hsu
The Hong Kong Polytechnic University
205 PUBLICATIONS **3,300** CITATIONS
SEE PROFILE

Journal of Aeronautics, Astronautics and Aviation, Vol. 55, No. 2, pp. 169 – 184 (2023)
*DOI: https://doi.org/10.6125/*JoAAA.202306_55(2).06

C/N_0 Assessment Based on GPS L5/L1C/A Signal Acquisition in Open-Sky/Light-Urban/Dense-Urban/Indoor Environments with Extended Coherent Integration Time *

Chin Lok Tsang [1], Yiran Luo [2] **, Bing Xu [1], and Li-Ta Hsu [1]

[1] *Department of Aeronautical and Aviation Engineering, The Hong Kong Polytechnic University, Hong Kong*
[2] *Department of Geomatics Engineering, University of Calgary, Calgary T2N1N4, Canada*

ABSTRACT

When the antenna receives the GNSS signals on the ground, the quality of the GNSS measurements will be closely related to the surrounding environment. Few works currently focus on comparing the performance of the legacy and the modern signals in the baseband signal processing level regarding different complicated environments. The paper proposed a long coherent integration algorithm for the GPS L1C/A and L5 signal performance comparison. Making use of the secondary code in the pilot channel of the L5 signal, an across-bit long coherent integration algorithm can be performed that minimizes the squaring loss and improves the signal-to-noise ratio (SNR). Then, with the aid of the bit edge estimated through the L5Q, a long coherent correlation can be directly performed in the L1C/A and L5I channels regardless of the unwanted bit change impact caused by the data symbol transition. The correlation powers are optimized for the legacy and the modern signal comparison in the acquisition process. The carrier-to-noise density ratio (C/N_0) and signal-acquired probability are used as the comparison index in the paper. A large scale of live sky IF data corresponding to different environments is collected for the experiment.

Keywords: Modernized GNSS, Code-Parallel acquisition, Long coherent integration, C/N_0 assessment, Urban canyon

I. INTRODUCTION

Global Navigation Satellite Systems (GNSS) gradually became inalienable in our daily lives and more advanced uses of GNSS such as GPS navigation for autonomous cars and mobile robots are expected soon. Anticipated the increasing demand and dependence on GPS in the future, the U.S Department of Defense launched the next-generation civil signal, L5, broadcast by GPS Block IIF in 2010. According to the National Coordination Office for Space-Based Positioning, Navigation, and Timing, GPS L5 is a third-generation signal aiming to improve civil users' navigation robustness and accuracy [1].

Three frequency-band signals, including L1, L2, and L5 are available in the GPS constellation. This paper would only focus on civilian L1C/A and L5 band signals transmitted by either block IIF or block III/IIIF satellites. Although the modernized GPS L2 band also contains the civilian L2C signal, its transmission power is lower than L5 band signals and the frequency is not within a reserved range. It is more likely to be affected by signal interference in environments with a similar frequency source. It is believed that L5 has a more advanced signal structure design and the greatest bandwidth, resulting in better signal processing sensitivity and navigation performance [2]. L5 would therefore be used for the comparison and representing the modernized GPS signal in the paper. Upon August 2022, there are 17 block IIF or GPS III/IIIF satellites transmitting L5 signal out of 31 satellites now in operation. BeiDou B2a and Galileo E5a signals also have very similar modulations and structures to the GPS L5

* Manuscript received, August 27, 2022, final revision, November 15, 2022
** To whom correspondence should be addressed, E-mail: yiran.luo@ucalgary.ca

signals, and the number of operational satellites of these two constellations are 27 and 22, respectively [3] [4]. Currently, many navigation satellites are transmitting new GNSS signals, and they are playing a vital role in the next-generation GNSS applications.

For the L1C/A and L5 signal performance comparison, literature is available that makes use of short and zero baseline analysis, which applies a geometry-free model and different linear combinations of GNSS measurements for separating the combination of different error sources to the measurement error at the receiver [5]. The work shows that L5 has revealed a lower thermal noise than L1, but strong variance had been shown from the pseudo-range code over an extended time interval [6]. It suggested that the phenomenon is most likely caused by severe short-range multipath combined with low multipath rejection by the antenna. The strong multipath variance may prevent the receiver from taking advantage of the high precision and advanced signal structure in L5. Another piece of literature accessed the L1C/A and L5 signals using 3D mapping aided (3DMA) to match the satellite visibility with the building boundary [7]. The multipath (M.P.) and non-line-of-sight (NLOS) effects are mitigated by using a traditional method that adjusted the GPS measurement weighting based on the C/N_0 and elevation angle provided by the receiver. The result suggested L5 has a better multipath resistance ability, but the performance is similar to the L1 band for the location with serve NLOS reception. Although, theoretically, L5 has a more advanced signal structure and is expected to provide better navigation performance, the result of their performance comparison may not be entirely consistent among different assessing methods. How the positioning performance using L5 signals are different from the L1C/A in various environments remains to be investigated in live sky tests. Therefore, other than the existing assessments, the paper assesses the L1 and L5 bands signals by revealing their performance from the perspective of signal processing.

The signal-to-noise ratio (SNR) is one of the most critical and direct indexes for determining the received signal quality. The higher the SNR is, the greater performance of the GNSS receiver behaves [8]. Usually, the SNR is expressed in terms of C/N_0 in the standard practice of GPS. It is the ratio between the signal power to noise power per unit bandwidth. Therefore, C/N_0 would be used for assessing the coarse navigation performance of L1C/A and L5 signals. This paper determines the C/N_0 in the acquisition stage corresponding to different time lengths of coherent integration, T_{coh}, including short, intermediate, and long coherent integration, which are defined to be T_{coh} < 10 ms, 10 ms ≤ T_{coh} ≤ 20 ms, and T_{coh} > 20 ms, respectively.

For weak signals, it has been suggested that extending the coherent integration time can effectively enhance signal detection and positioning performance [9] [10] [11]. The advanced signal structure of L5 provides the dataless L5Q channel which is born to make use of the long coherent integration. Since the Doppler frequency of the multipath signals would be different from the line-of-sight (LOS) signal, it will be separated or suppressed in the correlation process as explained by the synthetic aperture signal processing and pre-correlation suppression [12]. Multipath signals can be mitigated in the frequency domain with extended coherent integration time [10]. Therefore, long coherent integration is suggested in this paper for signal processing in challenging environments.

On the other hand, beneficial from the dataless feature of the L5Q channel, the data bit edge of L1C/A could be found by synchronizing it with the N.H. code edge searched from the L5Q channel. With the use of maximum likelihood estimation, the navigation data bits can be estimated in the no external adding condition, which helps the L1C/A achieve long coherent acquisition targeting weak signals conditions ignoring the impact from data bit transition. It would be beneficial for precise positioning in dual-frequency applications and also real-time carrier phase multipath detection [13].

Based on the above discussions, an experiment is conducted with live sky data to assess the L1C/A and L5 signals from the viewpoint of signal processing. Four different environments, including open-sky, indoor, light urban, and urban canyon, are chosen for comparison. The open-sky environment is used as a control setup for the signal comparison. The main contributions of this work are summarized as follows:

1. A long coherent code-parallel acquisition algorithm using the Fast Fourier transform (FFT) aided by the Neuman-Hofman (N.H.) code is proposed for the L5Q signal to improve the estimation accuracy and efficiency of the code phase and Doppler frequency.
2. A long coherent correlation algorithm is proposed in L1C/A and L5I acquisition aided by the N.H. code edge estimated from the L5Q signal.
3. A large scale of live sky intermediate-frequency (IF) GPS L5/ L1 CA data are collected from open-sky, light-urban, urban canyon, and indoor environments in Hong Kong for C/N_0 performance assessment in the signal acquisition level.

The paper is organized as follows. Section II discusses the signal model and characteristic differences between L1C/A, L5I, and L5Q. Understanding the signal structure, section III suggests the algorithm that makes use of the N.H. code edge searched out from L5Q for aiding L1C/A and L5I to perform long coherent integration removing the impact of unwanted bit transitions. Averaging C/N_0, acquired probability and C/N_0 standard deviation among trails would then be compared among the channels corresponding to different coherent integration times in section IV. The section will also discuss the potential reasons leading to the result.

II. GPS L1 AND L5 BAND SIGNAL MODEL AND CHARACTERISTIC

The structures between legacy L1C/A and modern L5 signals are greatly different. The section introduces the signal models and the signal characteristics for the GPS L1C/A and L5 band signals.

2.1 GPS L1 and L5 signal model

The GPS signals received by the receiver are the combination of signals transmitted by different satellites and white Gaussian noise. The intermediate frequency (IF) of the L1C/A signal, $y_{L1C/A}(nT_s)$, at the output of the radio frequency (RF) front-end can be expressed as follows for the line-of-sight (LOS) reception [14]:

$$y_{L1C/A}(nT_s) = A_{L1C/A}C(nT_s - \tau_0)d(nT_s - \tau_0)cos\big((\omega_{IF} + \omega_D)nT_s + \varphi_0\big) + \eta(nT_s) \quad (1)$$

where T_s is the sampling interval of the front end; n denotes the discrete-time sequence index; $A_{L1C/A}$ is the signal amplitude of L1C/A in LOS; τ_0 is the code delay; The navigation data, *d*, is modulated with the PRN code, *C*, and the carrier signal using the binary phase shift keying (BPSK) scheme. ω_{IF} and ω_D are the angular nominal IF frequency and Doppler frequency respectively; φ_0 is the initial phase of the carrier; $\eta(nT_s)$ is assumed to be the white Gaussian noise.

Different from L1C/A, the received L5 IF signal, $y_{L5}(nT_s)$, can be expressed as [15]:

$$y_{L5}(nT_s) = \Big\{\frac{1}{\sqrt{2}}A_{L5}C_{1,L5I}(nT_s - \tau_0)C_{2,L5I}(nT_s - \tau_0)d(nT_s - \tau_0)\,cos\big((\omega_{IF} + \omega_D)nT_s + \varphi_0\big)\Big\} + \{\tfrac{1}{\sqrt{2}}A_{L5}C_{1,L5Q}(nT_s - \tau_0)C_{2,L5Q}(nT_s - \tau_0)\,sin\big((\omega_{IF} + \omega_D)nT_s + \varphi_0\big)\} + \eta(nT_s) \quad (2)$$

where $L5I$ and $L5Q$ represent the in-phase data channel and the quadrature pilot channel respectively; A_{L5} is the total signal amplitude that combined $L5I$ and $L5Q$ channels; C_2 is the additional secondary code (N.H. code).

2.2 GPS L1 and L5 signal characteristics

The PRN code, carrier, and navigation data are the components modulated to form the legacy L1C/A signal. The PRN code of L1C/A is in a 1 ms period with a chipping rate of 1.023 MHz modulated with the carrier in 1575.42 MHz and navigation data bits at the rate of 50 bits per second (bps) using the modulo2 adder.

For the modern L5 signal, secondary codes (N.H. code) are modulated to the signals other than the PRN code, carrier, and navigation data. In terms of the PRN code, both the in-phase data channel and quadrature pilot channels are in a 1 ms period with a chipping rate of 10.23 MHz. It is expected that the increase in bandwidth of the L5 signal results in a shaper correlation peak. For the L5I data channel, unlike L1C/A, the navigation data at the rate of 50 bps is further processed with the ½ forward error correction (FEC) encoding resulting in a symbol rate of 100 sps [16]. The L5I N.H. code is modulated with the data symbols, carrier in 1176.45 MHz, and the PRN code with the modulo2 adder. For the L5Q pilot channel, the modulation is similar to L5I, but no navigation data element is involved [16]. Table 1 below summarizes the signal characteristics of L1C/A and L5 signals.

Table 1 Signal characteristics comparison of L1C/A and L5

		L1	L5	
Channel		Data - L1C/A	Data - L5I	Pilot - L5Q
Modulation		BPSK	BPSK	BPSK
Transmission frequency (MHz)		1575.42	1176.45	1176.45
Bandwidth (MHz)		2.046	20.46	20.46
Minimum received power (dW)		-158.5	-157.9 Block IIF -157.0 GPS III/IIIF	-157.9 Block IIF -157.0 GPS III/IIIF
Data rate (bps / sps)		50 / 50	50 / 100	NA
Primary Code (PRN code)	**Code rate (Mbps)**	1.023	10.23	10.23
	Period length (ms)	1	1	1
	Period length (code chips)	1023	10230	10230
Secondary Code (N.H. code)	**Code rate (bps)**	NA	1000	1000
	Period length (ms)	NA	10	20
	Code sequence	NA	[0000110101]	[00000100110101001110]

III. METHODOLOGY

Three stages are involved in C/N_0 estimation of the L1C/A and L5 channels by using the proposed algorithm that allows performing long coherent integration without unwanted bit change impact. The first stage is to search for the N.H. code edge in the L5Q channel. The edge would then be passed to L5I and L1C/A for aiding the long correlation implementation in the second stage. Finally, the C/N_0 estimation would be demonstrated in the third stage.

Stage 1: N.H. code edge searching

Both L1C/A and L5 signals use the same frequency source for code generation. The frequency source is 10.23 MHz, which fits the chipping rate of the primary code of the L5 signals. For L1C/A, a divider has been used that divides the frequency source by ten, which results in a 1.023 MHz frequency for L1C/A primary code generation. With the use of the same frequency source, the N.H. code edge of the L5 signal is therefore also the data bit edge of the L1C/A signal and they are synchronized.

This paper would not discuss the difference between the ionosphere delay of L1C/A and L5 as it is not the main contribution in this work. Based on the assumption that both L1 and L5 signals reach the ground at nearly the same time, the L5Q pilot signal could achieve parallel-code search (PCS) acquisition with the discrete Fourier transform. In general, the FFT would be used to speed up the correlation between the replica and the incoming signal in the frequency domain [17]. IFFT is then used to reverse the transform back to the time domain and find out the signal peak. The algorithm is widely used by most commercial receivers nowadays [18]. It provides the benefit of less memory requirement, a high level of parallelism, and precise Doppler compensation [19]. As the N.H. code period is 20 ms, it is crucial to ensure the retrieved incoming signal interval as an integer multiple of the N.H. code period for forming a maximum power peak over the cross-correlation process [15]. The cross-correlation of the incoming signal and the replica is shown in Figure 1, where y_{L5Q}, R_{L5Q} and N are the L5Q IF signal, L5Q replica and total number of samples within the chip respectively.

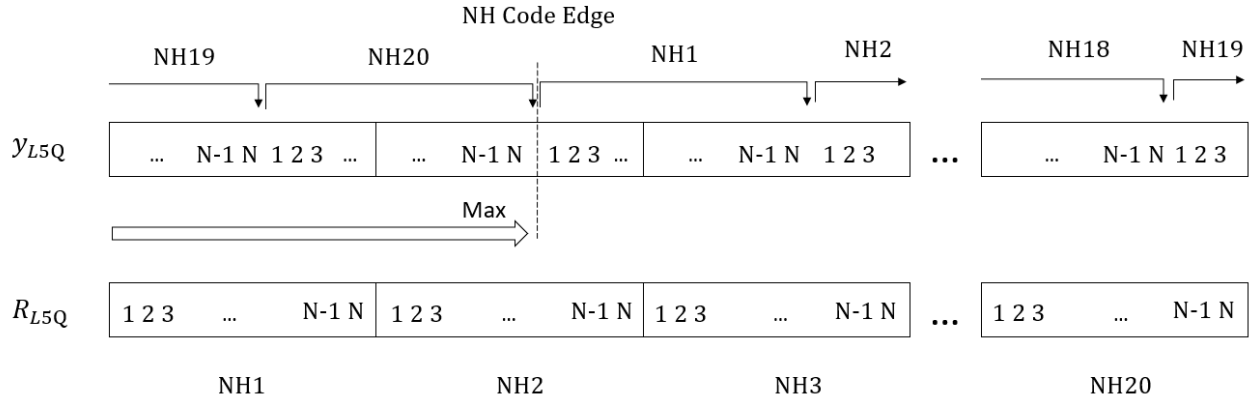

Figure 1 Incoming IF signal and replica in the cross-correlation process

Figure 2 shows the PCS algorithm used on L5Q for edge finding. A randomly chosen coherent integration length, 40 ms, is used as an example for demonstrating the algorithm. A 40 ms long replica containing 40 cycles of PRN codes and 2 cycles of 20-bit N.H. code, would be used for performing cross-correlation to search for the N.H. code edge. If the required coherent integration time is not in the multiple of 20 ms, it would be rounded up to an integer multiple of 20 ms for processing. The serial search process is adopted for the Doppler frequency estimation in the acquisition. The search step is set as $f_{d_s} = \frac{2}{3\ T_{coh}}$ [20], where T_{coh} is the coherent integration time. For the 40 ms coherent integration case, $f_{d_s} = 16.67\ Hz$. It starts searching from $f_{IF} - 5000$ Hz to $f_{IF} + 5000$ Hz. The correlation result corresponding to different Doppler steps can be represented in the matrix form, $A_{\mathrm{L5Q,corr}}$:

$$A_{\mathrm{L5Q,corr}} = \begin{bmatrix} A_{L5Q,1,1} & \cdots & A_{L5Q,1,n1} \\ \vdots & \ddots & \vdots \\ A_{L5Q,i_{\max},1} & \cdots & A_{L5Q,i_{\max},n1} \end{bmatrix} \quad (3)$$

where $i_{\max}$ is the number of Doppler steps involved in the search range; n_1 is the number of samples within the incoming signal used for cross-correlation. The elements in the matrix, $A_{L5Q,row\ index,column\ index}$, are the signal amplitude corresponding to different code phases and doppler values under the envelope of $\sqrt{I^2 + Q^2}$.

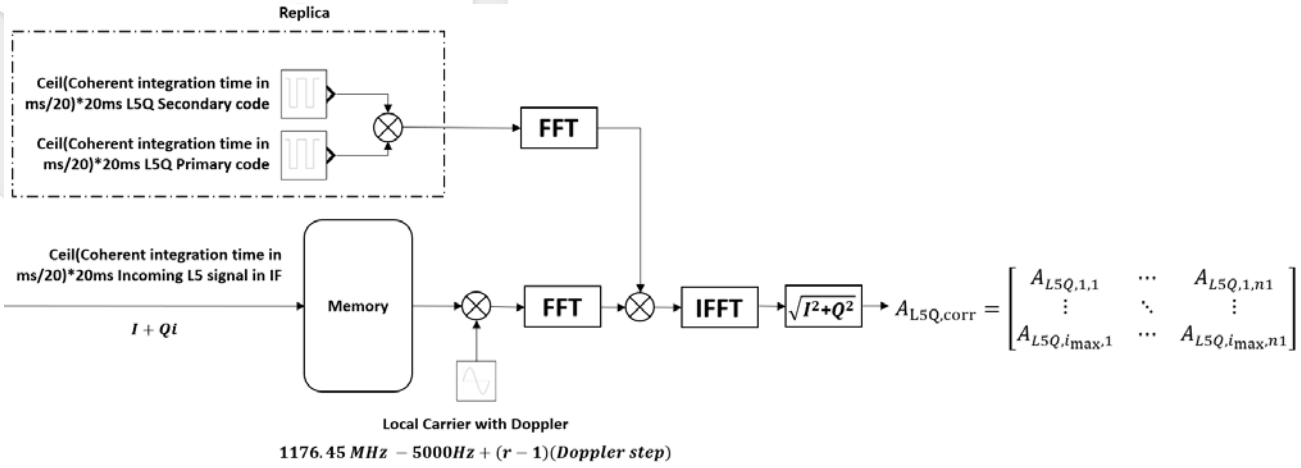

Figure 2 N.H. code edge searching with the use of the L5Q channel

The cross-ambiguity function corresponding to I and Q correlation can be expressed as [11]:

$$Y(\hat{\tau},\hat{\omega}_D) = \sqrt{Y_I(\hat{\tau},\hat{\omega}_D)^2 + Y_Q(\hat{\tau},\hat{\omega}_D)^2} \quad (4)$$

Where

$$Y_I(\hat{\tau},\hat{\omega}_D) = \sum_{n=1}^{n_1} y_{L5}(nT_s)C_{1,L5Q}(nT_s-\hat{\tau})C_{2,L5Q}(nT_s-\hat{\tau})\cos\left[\left(\omega_{IF,L5Q}+\hat{\omega}_D\right)nT_s\right] \quad (5)$$

$$Y_Q(\hat{\tau},\hat{\omega}_D) = \sum_{n=1}^{n_1} -y_{L5}(nT_s)C_{1,L5Q}(nT_s-\hat{\tau})C_{2,L5Q}(nT_s-\hat{\tau})\sin\left[\left(\omega_{IF,L5Q}+\hat{\omega}_D\right)nT_s\right] \quad (6)$$

$\hat{\tau}$ and $\hat{\omega}_D$ denote the estimated local replicated code delay, and estimated Doppler frequency, respectively. The element with the maximum magnitude is searched within $A_{\mathrm{L5Q,corr}}$:

$$\left[n_{Edge},\hat{f}_g\right] = \mathrm{argmax}\left\{\left|A_{\mathrm{L5Q,corr}}\right|^2\right\} \quad (7)$$

where n_{Edge} is the discrete-time sequence index for the sample closest to the absolute edge of the signal; $\hat{f}_g$ denotes the coarse estimated Doppler frequency corresponding to the search. With the N.H. code edge position being found, the possible data bit transition impact on coherent integration can be removed using the maximum likelihood bit estimation method. Coherent integration can be performed at an extended time length that would increase the weak signal acquired probability in a degraded environment [9] [10] [11].

Stage 2: L1C/A, L5I and L5Q correlation corresponding to different coherent integration times

The discrete-time sequence index for the sample closest to the absolute edge of the signal, n_{Edge}, searched in Stage 1 is passed to L1C/A and L5I for aiding their long coherent correlation. Figure 3, Figure 4, and Figure 5 show the long correlation algorithms of L5Q, L5I, and L1C/A, respectively. The algorithm fits any coherent integration time and gets rid of unwanted bit transition impact. The replica containing PRN code and N.H. code is circularly shifted by $(n_{\mathrm{Edge}}-1)$ for synchronizing the edge. For L5Q, local samples of the circularly shifted replica are directly multiplied with incoming signal samples for signal correlation and the demodulated signal is then added up. For L5I and L1C/A, an additional bit estimation procedure had been added compared with the correlation algorithm of the L5Q pilot channel. The symbol rate of navigation data are in 100 sps and 50 sps for L5I and L1C/A, respectively. The symbol transition may happen in 10 ms and 20 ms for L5I and L1C/A respectively. A serial search would be performed in symbol bit estimation that tries different symbol combinations accordingly and searches for the one best fits the incoming signal. The total number of the bit sign combination can be represented as $d_{L1C/A}$ and d_{L5I} corresponding to L1C/A and L5I as follows.

$$d_{L1\ C/A} = 2^{ceil\left(\frac{T_{coh}}{0.02}\right)+1} \quad (8)$$

$$d_{L5I} = 2^{ceil\left(\frac{T_{coh}}{0.01}\right)+1} \quad (9)$$

Continuing the 40 ms coherent integration case brought up in section 3.1 as an example, the total number of symbol combinations in L1C/A is $2^{ceil\left(\frac{0.04}{0.02}\right)+1} = 8$. Possible data symbol combinations for the signal are [-1,-1,-1], [-1,-1,1], [-1,1,-1], [-1,1,1], [1,-1,-1], [1,-1,1], [1,1,-1], and [1,1,1]. However, only the first half combinations would undergo serial search accordingly as the correlation result of the combination [-1,-1,-1], [-1,-1,1], [-1,1,-1], and [-1,1,1] would be the same as [1,1,1], [1,1,-1], [1,-1,1], and [1,-1,-1], respectively, under the envelope of $\sqrt{I^2+Q^2}$. The replica is formed after the data symbol combinations are modulated with the primary code of L1C/A or primary code & secondary code of L5I. They are then circularly shifted toward the n_{Edge} position and perform

correlation. The highest signal amplitude would be formed when the data symbol is correctly estimated. With the data symbol, coarse code phase, and coarse Doppler frequency being found, a fine search with 1 Hz Doppler steps is performed for the precise Doppler frequency estimation.

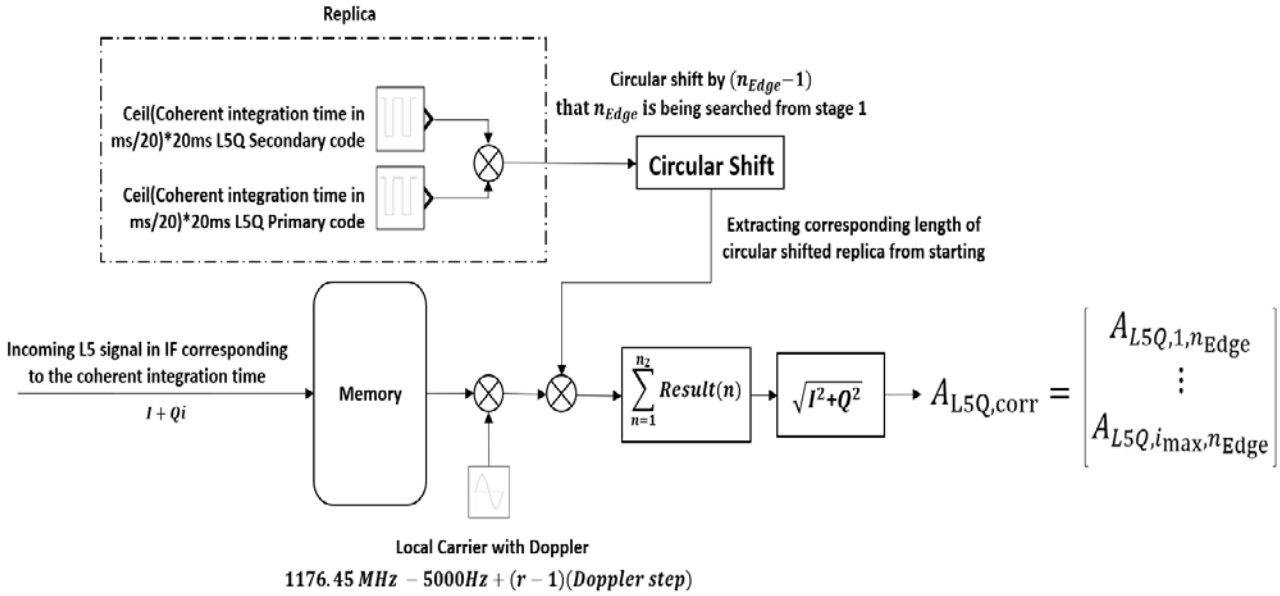

Figure 3 Direct correlation process of L5Q corresponding to different coherent integration times

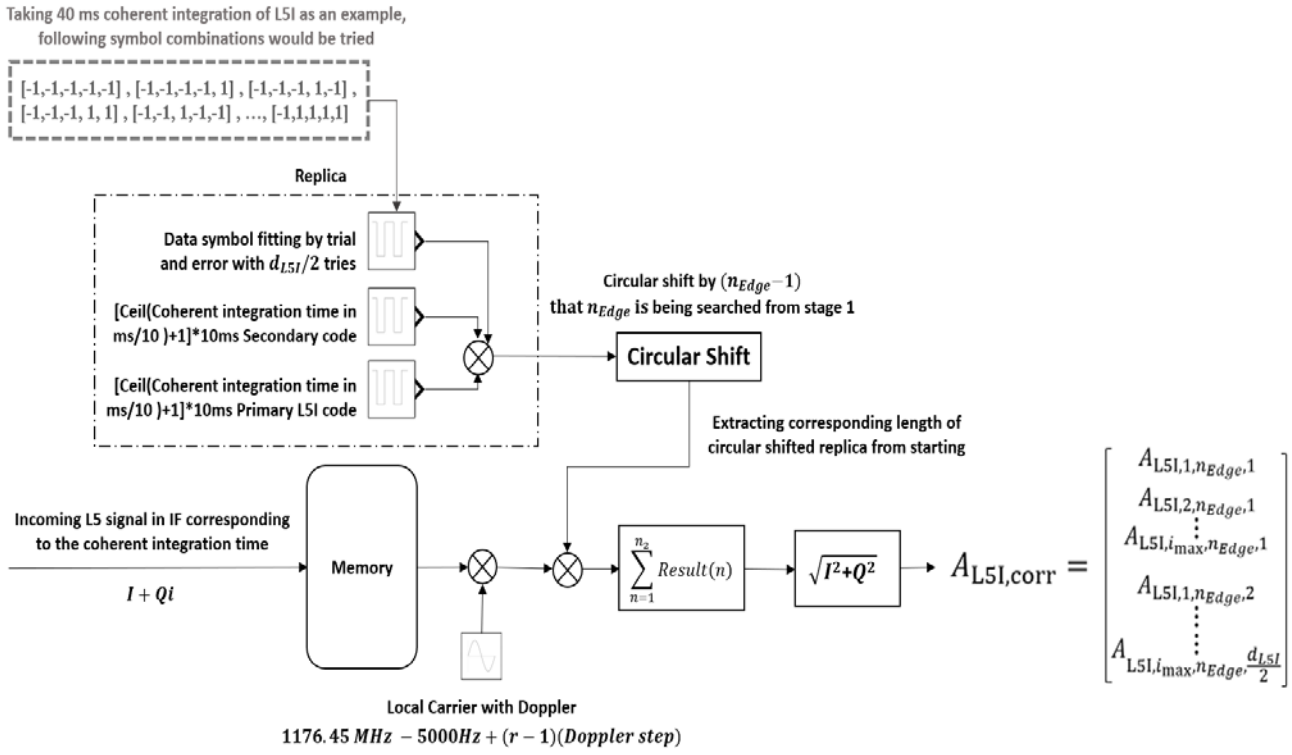

Figure 4 Direct correlation process of L5I corresponding to different coherent integration times

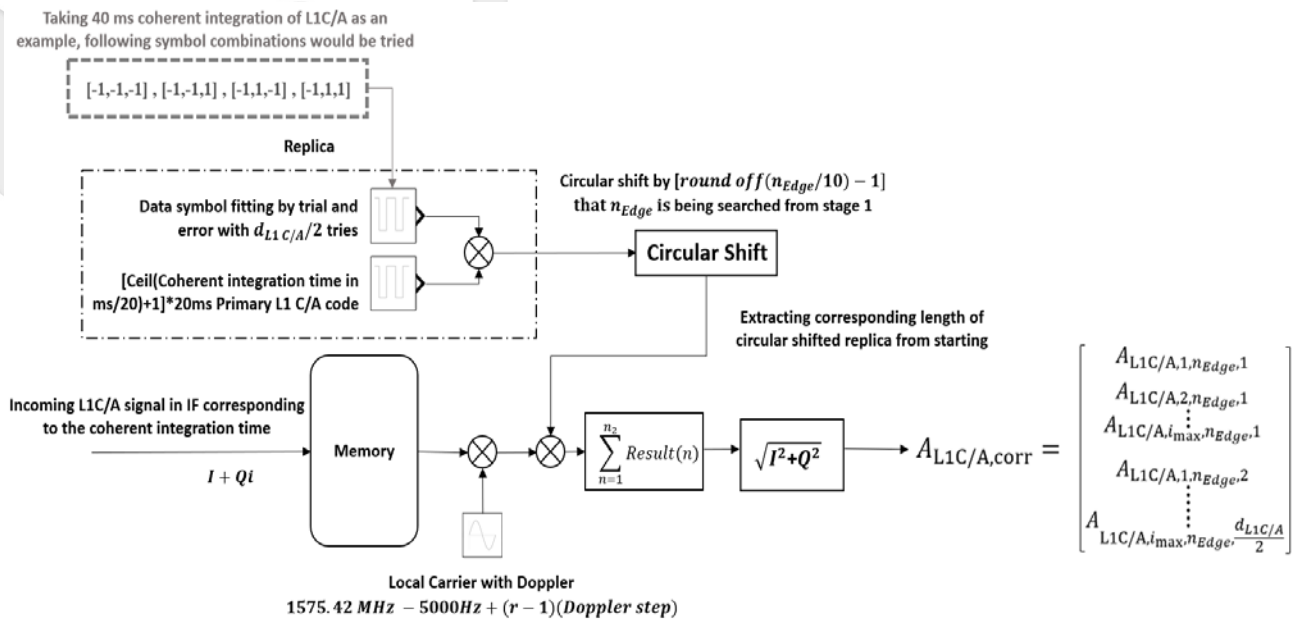

Figure 5 Direct correlation process of L1C/A corresponding to different coherent integration times

Stage 3: C/N_0 estimation

The correlation result and the peak formed in Stage 2 are under the envelope of $\sqrt{I^2+Q^2}$. The envelope follows the Rician distribution while I and Q are in the Gaussian distribution when satellite signals are present [21]. If there is no signal but only noise, the envelope would be in Rayleigh distribution.

In the experiment, the probability of fault alarm, P_{fa}, is set to 10^{-6}. When the amplitude of the correlated signal exceeds or is equal to V_t, a signal would be declared as presence. Otherwise, it will announce that no signal is being detected. The noise amplitude, σ_n, can be found by forming a noise channel through an unused PRN code (PRN 35 was used in the case) correlating with the incoming IF signal. Knowing that the white Gaussian noise is in a Rayleigh distribution under the envelope of $\sqrt{I^2+Q^2}$, it can be found by the Rayleigh property. The threshold for signal detection is:

$$V_t = \sigma_n\sqrt{-2\ln P_{fa}} \tag{10}$$

The noise amplitude is computed as:

$$\sigma_n = \frac{mean\ value\ of\ noise\ channel}{\sqrt{\frac{\pi}{2}}} \tag{11}$$

Knowing the σ_n, the signal-to-noise ratio, SNR_{Hz}, and carrier-to-noise ratio, $C/N_{0\ dB}$ can be found by:

$$SNR_{Hz} = \frac{A^2}{2\sigma_n^2} \tag{12}$$

$$C/N_{0\ dB} = 10\log(SNR_{Hz}) - 10\log(\ T_{coh}) \tag{13}$$

IV. EXPERIMENTAL RESULTS AND DISCUSSION

Two sets of live sky data at the same location but at different times were collected for the acquired probability and C/N_0 assessment. The skyplot of the datasets is shown in Figure 6.

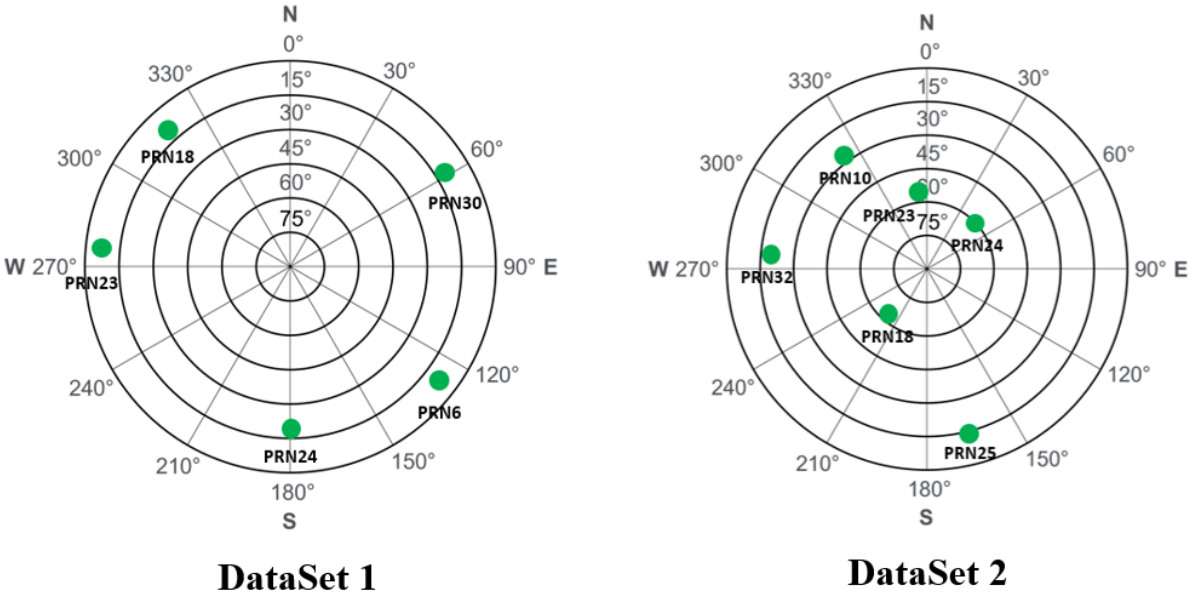

Figure 6 Skyplot of the datasets

4.1 Live sky environments and experimental setup

GPS L1 and L5 band signals are collected in the open-sky, indoor, light urban, and dense urban environments with the use of the LabSat3 wideband. The locations corresponding to the environments are the peak of Sai Ko Shan (22°16'20.5"N 114°08'10.5"E), Fortune Metropolis in Hung Hom (22°18'08.9"N 114°11'00.3"E), a crossroad in Whampoa (22°18'20.3"N 114°11'19.2"E), and a tram stop in Central (22°17'00.5"N 114°09'23.5"E), respectively. Figure 7 shows the environments surrounded by the signal collection point. The peak of Sai Ko Shan is only a relatively open-sky environment as there are slightly higher peaks nearby which may cause multipath effects and obstruct the signal transmission of low-elevation angle satellites.

Figure 7 Surrounding environment of the signal collection points

GPS satellites are flying in Medium Earth Orbit (MEO) and the satellites have a nominal period of 11 hours 58 minutes 2 seconds. The set of data that involves signals in four different environments is collected on four consecutive days. The signal would be collected with a time separation of 23 hours 56 minutes (2 MEO period) to ensure the elevation angle of the satellites remains the same at different signal collection locations. It keeps the elevation angle independent for assessing the L1C/A and L5 signal performance in different environments.

Both sets of data contain four environments. The first set of data mainly targets low-elevation and medium-elevation angle satellites, and the second set of data is majorly targeting medium elevation angle and high-elevation-angle satellites.

Figure 8 shows the data collection setup. A high-precision GPS antenna, GPS-703-GGG-HV, with excellent multipath rejection capability is used for L1 and L5 band signal reception. A splitter is used to split the signal into two and feed it to the LabSat3 wideband and ublox C099-F9P application board respectively. The parameter settings of the LabSat3 Wideband used in the experiment are listed in Table 2. The LabSat3 wideband heterodynes the satellite signals and downconverts them into IF for SDR processing. Another spitted signal is fed into the ublox C099-F9P application board to evaluate the elevation angle of the overhead satellites for reference.

The chipping rate of the L5 PRN code is 10.23 MHz, which is ten times of L1C/A. Therefore, the experiment down-sampled the L1C/A signal to 5.8 MHz for correlation that ensured the signals contain the same number of samples within a chip and can neglect the potential error caused by ambiguous synchronization.

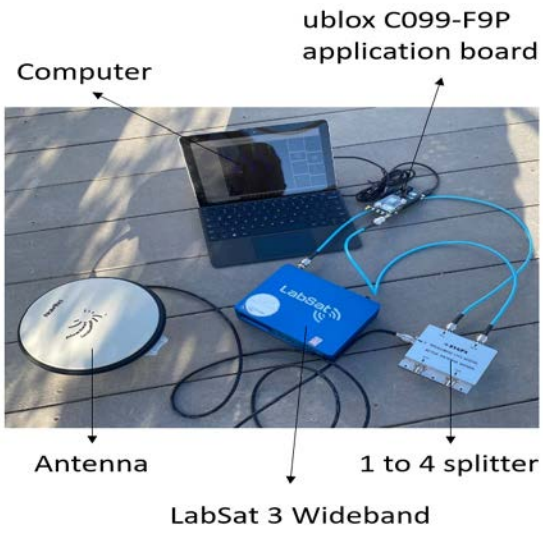

Figure 8 Experimental set-up

Table 2 LabSat3 Wideband parameter settings

Signal type	**GPS L1C/A**	**GPS L5**
IF sampling rate	58 MHz (down-sampled to 5.8 MHz for the SDR acquisition algorithm processing)	58 MHz
Center frequency	1580 MHz	1191.795 MHz
Quantization type	2 bits and complex form	
Coherent integration time at Stage 1	20 ms/ 40 ms	
Coherent integration time at Stage 2	1, 2, 5, 10, 20, 40 ms	
Front-end oscillator	Oven-Controlled Crystal Oscillator (OCXO)	

4.2 Satellite elevation angle

For satellite with an elevation angle between 0°and 20°, it is considered a low elevation angle. In the case of $20° \leq$ Elevation Angle $< 40°$, it is defined as a medium elevation angle. Finally, satellites belong to the class of high elevation angle when $40° \leq$ Elevation Angle $\leq 90°$. Based on the datasets, 100 trials had been run for L1C/A, L5I, and L5Q channels corresponding to the coherent integration time of 1 ms, 2 ms, 5 ms, 10 ms, 20 ms, and 40 ms. The averaging C/N_0 has been taken among the 100 trials for signal performance comparison. Other than the averaging C/N_0, the acquired probability and C/N_0 standard deviation are being compared among the channels. Table 3 lists satellite elevation angles corresponding to the datasets. The results of PRN 18 in dataset 1 with a low elevation angle, PRN 11 in dataset 1 with a medium elevation angle, and PRN 18 in dataset 2 with a high elevation angle would be taken as an example for the subsequent discussions.

Table 3 Satellite elevation angle corresponding to the two sets of data.

Data	Environment	PRN	Elevation Angle (°)	
Set 1	Open-Sky	6	Low	9
		18		12
		23		7
		24		18
		30		12
		11	Med	34
	Light Urban	11	Med	34
	Dense Urban	11	Med	34
	Indoor	18	Low	12

Data	Environment	PRN	Elevation Angle (°)	
Set 2	Open-Sky	25	Low	14
		10	Med	28
		32		20
		18	High	64
		23		55
		24		46
	Light Urban	10	Med	28
		18	High	64
		23		55
		24		46
	Dense Urban	10	Med	28
		18	High	64
		23		55
		24		46
	Indoor	18	High	64

4.3 Acquired Probability

Satellites at low elevation angles are the most challenging case among the environments and would be discussed regarding the acquired probability. The acquired probability is found by the number of experimental trials with signal amplitude passed the detection threshold V_t out of all the experimental trials. Regarding satellite with PRN 18, no signal could be detected in the light urban and dense urban environments. As shown in Figure 9, for the open-sky and indoor environments, the acquired probability of L5I and L5Q closely align corresponding to different coherent integration times. The result suggested that they are in ideal quadrature phase-shift keying (QPSK) modulation and embrace very similar acquisition performance in the GNSS baseband signal processing.

The acquired probability increase with extended coherent integration time for both L5 and L1C/A channels. For L5 channels, the increase in acquired probability corresponding to extended coherent integration time is more rapid in the open-sky environment than in the indoor environment. For L1C/A, no signal can be detected among all the trials in 1 ms and 2 ms coherent integration in the open-sky environment since the signal amplitude cannot pass the detection threshold. In the indoor environment, no signal can be detected even if the coherent integration time is extended to 40 ms. The signal power of L1C/A is hard to penetrate and reach the indoor environment in this case and resulting in an extremely weak signal. The result suggested that L5 band signals are superior to L1C/A in terms of acquired probability. They provide higher received power, excellent resistance to the white Gaussian noise, and are more likely to be detected than L1C/A.

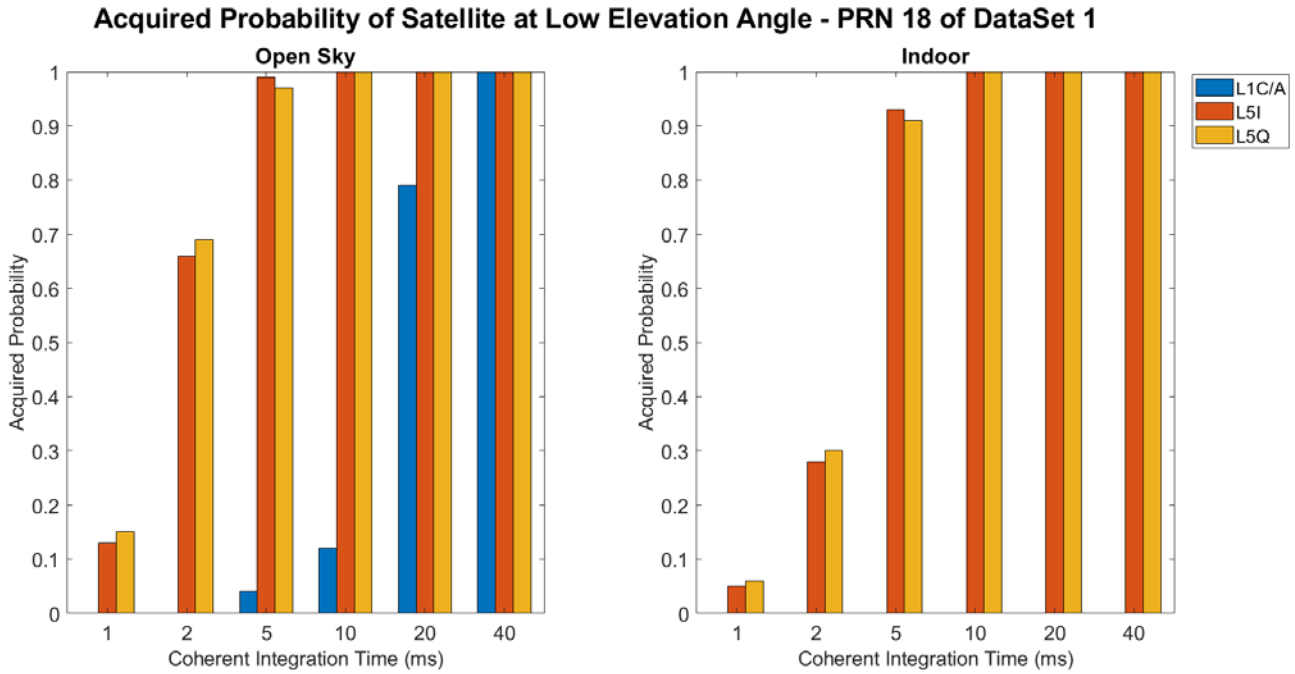

Figure 9 Acquired probability of satellite at low elevation angle

4.4 Averaging C/N_0

The averaging C/N_0 of satellites at high, medium and low elevation angles are shown in Figure 10, Figure 11, and Figure 12 respectively.

For satellites at high elevation angles, the received signal is less likely to be affected by NLOS interference. Figure 10 shows that the averaging C/N_0 of L5I and L5Q have a similar magnitude and the averaging C/N_0 of L1C/A corrosponding to different coherent integration

times are lower than L5I and L5Q in all environments when a satellite is at a high elevation angle. No blue bars appear in 1 ms and 2 ms coherent integration in the open-sky, light urban and dense urban environment. The disappearance of bars means the signal's acquired probability is lower than 0.5 and less than 50 out of 100 trials with a signal being detected, therefore results corresponding to the coherent integration time are being ignored in the plotting as there are too few successful trials to account for the averaging C/N_0. The averaging C/N_0 difference between the L5 signals and L1C/A are very similar in open-sky, light urban and dense urban environments. In the high elevation angle condition, the averaging C/N_0 difference can be explained by the greater transmission power of L5 results in a higher received power of the receiver. For the indoor environment, the acquired probability of the L1C/A signal is lower than 0.5 even if the coherent integration time is extended to 40 ms. This happens due to the presence of a very weak signal. However, bars only disappear in 1 ms for L5I and L5Q in the indoor environment. The acquired probability is over 0.5 as of 2 ms coherent integration. Other than a higher power is required for the satellite signal to penetrate the glass and reach the antenna in the indoor environment, the signal highly depends on the diffraction property to overcome the obstacles blocking the signal's line of sight and reach the indoor antenna. The degree of diffraction is proportional to the wavelength under the same transmission media [22]. The L5 signals have a longer wavelength than L1C/A, and they have better diffraction properties which are superior to L1C/A in the indoor environment.

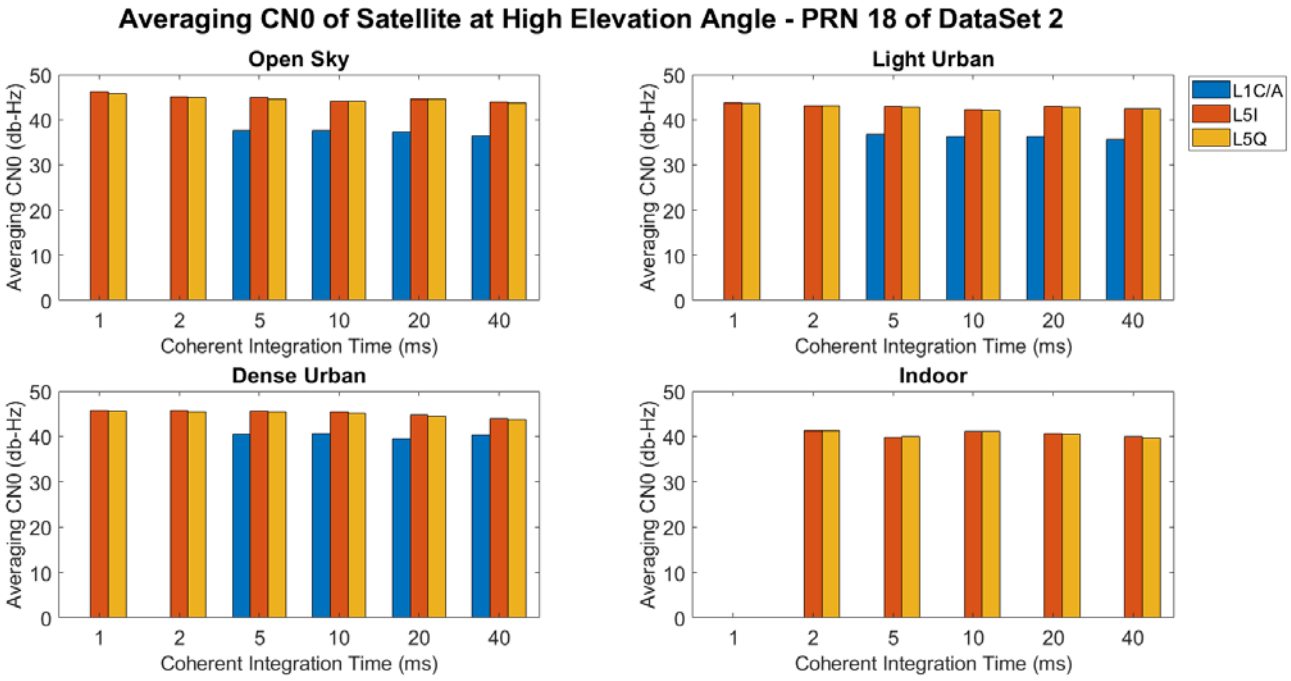

Figure 10 Averaging C/N_0 of satellite at high elevation angle

For satellite at medium elevation angle, Figure 11 shows signals can be detected in open-sky, light urban and dense urban environments, but not in the indoor environment. Again, the averaging C/N_0 of L5I and L5Q are close to each other and they have a higher magnitude than the L1C/A when a satellite is at the medium elevation angle. The buildings in light urban are dense but relatively short. Satellite signals are relatively easy to be diffracted to reach the antenna. Greater transmission power would be the dominant reason resulting in a higher averaging C/N_0 of L5 than L1C/A. For the dense urban, it is a more challenging environment where the tall and dense buildings would obstruct the signals transmitted by medium elevation angle satellites. Points disappear in 1 ms, 2 ms. 5 ms and 10 ms coherent integration of L1C/A, but points only disappear in 1 ms, 2 ms and 5 ms coherent integration of L5 channels; It demonstrates the L5 signals have a better reflection property under a greater transmission power in the NLOS environment. The L5 signals are more robust than L1C/A in a dense urban environment.

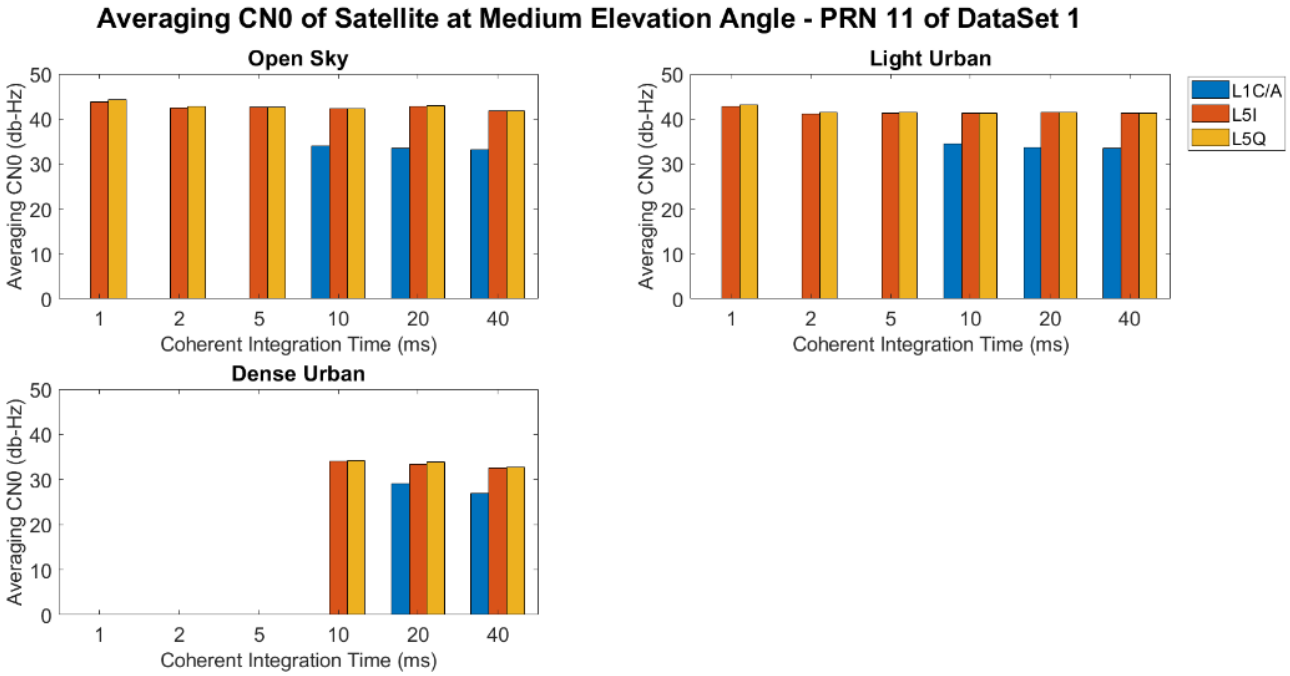

Figure 11 Averaging C/N_0 of satellite at medium elevation angle

For satellite at low elevation angle, Figure 12 shows signals can only be detected in the open-sky and indoor environments, but not the light urban and dense urban. As mentioned, the experimental environment is only relatively open-sky, slightly higher peaks nearby obstruct the signal transmission of the low elevation angle satellite or reflect the signals resulting in a multipath situation. When the signal is blocked by the higher peaks and in the NLOS situation, L5 channels have a better diffraction property and greater transmission power as previously mentioned. In the multipath situation, L5 signals have a wider bandwidth that could better suppress or mitigate the multipath signal in the cross-correlation. The multipath signal peak could separate out with a greater signal bandwidth. The LOS signal experiences less degradation and attenuation caused by the reflected multipath signal. Under better diffraction property, greater transmission power and advanced signal structure resulting in better multipath resistance, L5 signals have a higher averaging C/N_0. Also, a shorter coherent integration time is required for signal detection. In the indoor environment, no L1C/A signal can be detected even the coherent integration time is extended to 40 ms. However, for L5I and L5Q, signals can be detected and the acquired probability is over 0.5 as of 2 ms coherent integration. This further proved that L5 signals are superior to L1C/A in the indoor environment.

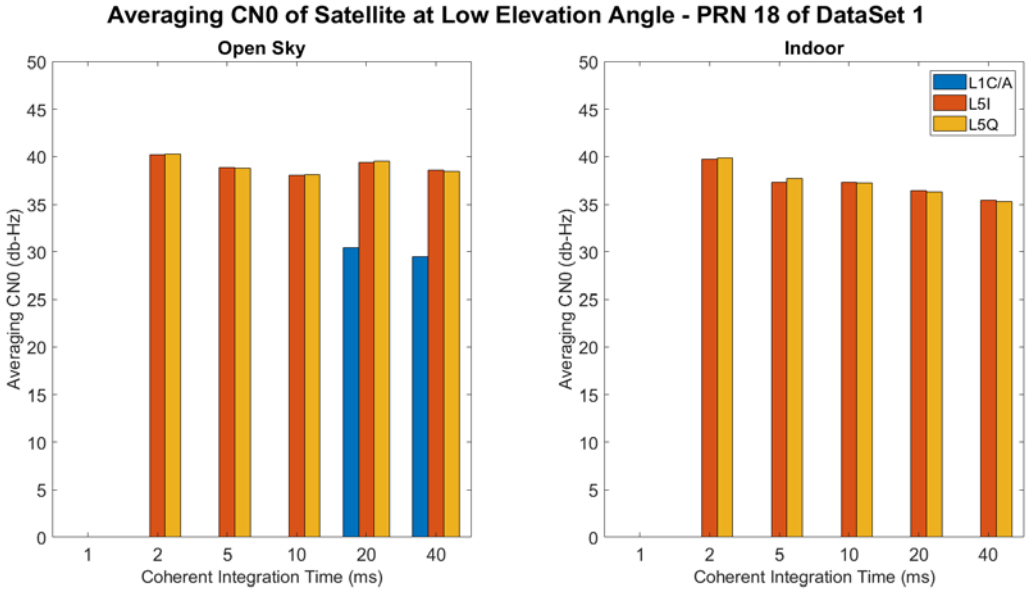

Figure 12 Averaging C/N_0 of satellite at low elevation angle

To sum up, no matter at high, medium and low elevation angles, the L5I and L5Q has a higher averaging C/N_0 than L1C/A in all environments. On the other hand, as L5 channels for weak signal detection require a shorter integration time interval, it demonstrates L5 is superior to L1C/A in the application where the long coherent integration is exploited to overcome the challenging environments in navigation. Finally, there are some unified laws for all the signals: at first, the longer the coherent integration time is, the lower the averaging C/N_0 becomes. As the satellite keeps moving but the local code generated did not account for the factor of satellite movement, when synchronizing the local code with the edge of the incoming signal, the impact from the satellite dynamic will increase with extended coherent integration time and resulting in a decrease in C/N_0. Moreover, the bars corresponding to L5I and L5Q are closely aligned. It further shows that they are in an ideal quadrature phase-shift keying (QPSK) modulation. They embrace very similar performances in terms of the GNSS baseband signal processing.

4.5 C/N_0 standard deviation

Other than the acquired probability and averaging C/N_0 and, the C/N_0 standard deviation among trials are compared between the L1C/A and L5 signals. The C/N_0 standard deviation of satellite with a high elevation angle in the open-sky environment would be sequentially discussed. Figure 13 shows the C/N_0 standard deviation of satellite at high elevation angle in the open-sky environment. The signal's detection probability is lower than 0.5 for 1 ms and 2 ms coherent integration of L1C/A and the C/N_0 standard deviation results are being ignored correspondingly due to too few trials that could be used to account for the statistic. Both L1C/A and L5 signals are in a gently decreasing trend with extended coherent integration time. It shows the signals become more stable with extended coherent integration time. On the other hand, the C/N_0 standard deviation of L1C/A always locate below L5 as of 5 ms coherent integration. The chipping rate of L1C/A is 1.023 Mbps, which is ten times lower than 10.23 Mbps of L5 signals. The L1C/A is less sensitive to the satellite dynamic due to a narrower bandwidth and has a lower C/N_0 standard deviation.

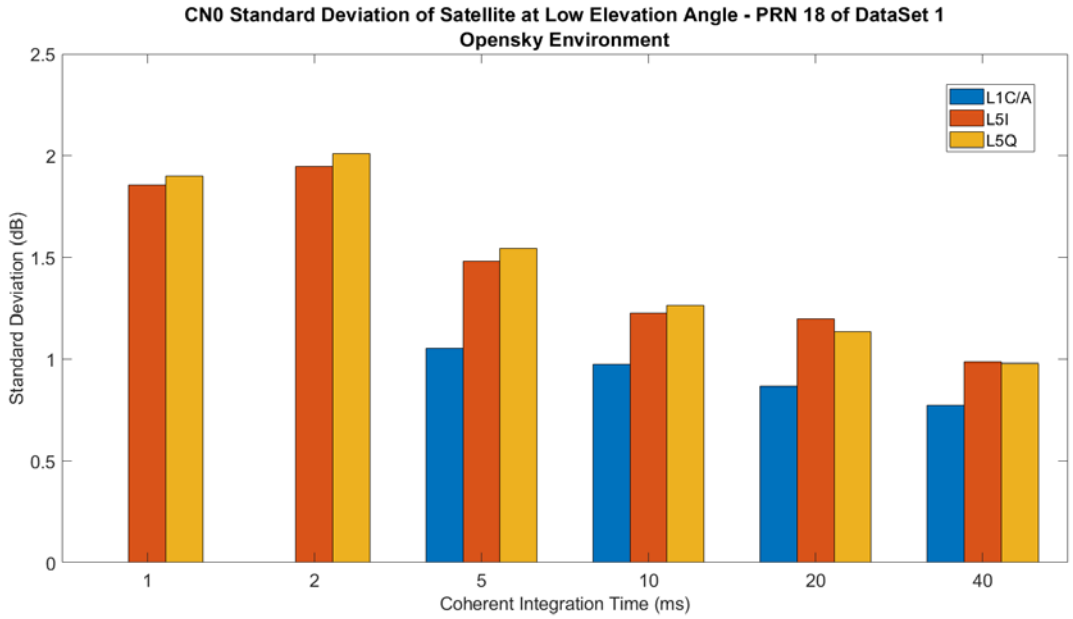

Figure 13 C/N_0 standard deviation of satellite at high elevation angle in the open-sky environment

4.6 Coherent and non-coherent integration

The above parts have shown the L5 signals are superior to L1C/A corresponding to different environments with an extended coherent integration time under the proposed algorithm. However, the signal performance between the extended coherent integration and non-coherent integration has not yet been shown. In this part, coherent integration and non-coherent integration with 1 ms coherent interval of the L5Q channel would be compared sequentially and the relatively open-sky environment with satellite in high elevation angle condition would be used for comparison.

The general decreasing trend of both the coherent and non-coherent integration could be summarized as the satellite dynamics as discussed previously. However, it can be observed the decreasing trend is more rapid with a longer integration time in the non-coherent case. With more numbers of 1 ms coherent intervals being added up, a greater squaring loss is resulted. When extended toward 40 ms integration, the coherent and non-coherent difference in terms of averaging C/N_0 is about 2 dB-Hz in the test case. The result demonstrates that extended coherent integration provides a much better signal performance and greater noise resistance compared with non-coherent integration. The reduction in squaring loss allows the signal to stand out in the weak signal condition and will be beneficial in a challenging environment.

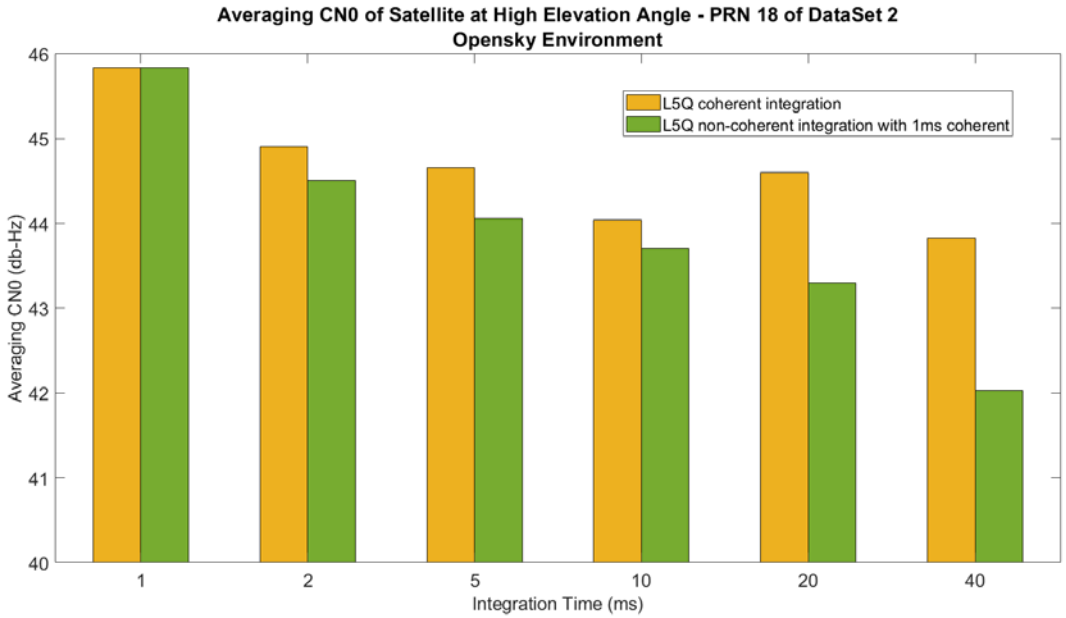

Figure 14 Averaging C/N_0 of coherent and non-coherent integration

V. CONCLUSIONS

The paper has assessed the acquisition performances of the GPS L1C/A and L5 signals by comparing the averages and standard deviations of the C/N_0 estimations as well as the acquired probability in four typical environments in Hong Kong. Conclusions can be drawn from the experimental results: firstly, the L5 signals are more advanced to improve the C/N_0 in challenging environments by taking advantage of the long coherent integration. On the other hand, both the detection probability and stability in acquisition for L5 signals are higher than the L1 C/A signal, especially in a challenging environment. However, the C/N_0 estimation of L1 C/A signals based on a long coherent integration is less sensitive to the signal dynamics than the L5 signals. Finally, the L5Q and L5I embrace very similar performances in the GNSS baseband signal processing.

ACKNOWLEDGMENTS

This research is supported by the University Grants Committee of Hong Kong under the scheme Research Impact Fund on the project R5009-21 “Reliable Multiagent Collaborative Global Navigation Satellite System Positioning for Intelligent Transportation Systems”.

REFERENCES

[1] “GPS.gov: New Civil Signals,” 2020. https://www.gps.gov/systems/gps/modernization/civilsignals/ (accessed Feb.15, 2022).

[2] Tran M, “Performance evaluations of the new GPS L5 and L2 Civil (L2C) signals,” *Navigation, Journal of the Institute of Navigation*, Vol. 51, No. 3, 2004, pp. 199-212. doi: 10.1002/j.2161-4296.2004.tb00351.x.

[3] “Constellation Information,” European GNSS Service Centre, 2021. https://www.gsc-europa.eu/system-service-status/constellation-information (accessed Feb.15, 2022).

[4] “Constellation Status,” Test and Assessment Research Center of China Satellite Navigation Office, 2021. http://www.csno-tarc.cn/en/gps/constellation (accessed Feb.15, 2022).

[5] deBakker PF, van derMarel H, Tiberius CCJM, “Geometry-free undifferenced, single and double differenced analysis of single frequency GPS, EGNOS and GIOVE-A/B measurements,” *GPS Solutions*, Vol. 13, No. 4, 2009, pp. 305-314. doi: 10.1007/s10291-009-0123-6.

[6] deBakker PF, Tiberius CCJM, van derMarel H, vanBree RJP, “Short and zero baseline analysis of GPS L1 C/A, L5Q, GIOVE E1B, and E5aQ signals,” *GPS Solutions*, Vol. 16, No. 1, 2012, pp. 53-64. doi: 10.1007/s10291-011-0202-3.

[7] Ng HF, Zhang G, Yang KY, Yang SX, Hsu LT, “Improved weighting scheme using consumer-level GNSS L5/E5a/B2a pseudorange measurements in the urban area,” *Advances in Space Researc*h, Vol. 66, No. 7, 2020, pp. 1647-1658. doi: 10.1016/j.asr.2020.06.002.

[8] Groves PD, “GPS signal-to-noise measurement in weak signal and high-interference environments,” *Navigation, Journal of the Institute of Navigation*, Vol. 52, No. 2, 2005, pp. 83-94. doi: 10.1002/j.2161-4296.2005.tb01734.x.

[9] Watson R, Lachapelle G, Klukas R, “Investigating GPS Signals Indoors with Extreme High-Sensitivity Detection Techniques,” 2006.

[10] Pany T, Reidl B, Winkel J, Worz, T., andSchweikert, R., "Coherent Integration Time: The longer, the better," InsideGNSS, 2009, pp. 52-61.
[11] Borio D, O'Driscoll C, Lachapelle G, "Coherent, noncoherent, and differentially coherent combining techniques for acquisition of new composite GNSS signals," *IEEE Transactions on Aerospace and Electronic Systems*, Vol. 45, No. 3, 2009, pp. 1227-1240.
doi: 10.1109/TAES.2009.5259196.
[12] Xie P, Petovello MG, "Improving high sensitivity receiver performance in multipath environment for vehicular applications," 25th International Technical Meeting of the Satellite Division of the Institute of Navigation 2012, ION GNSS 2012, Vol. 1, No. April, 2012, pp. 448-457.
[13] Zhang Z, Li B, Gao Y, Shen Y, "Real-time carrier phase multipath detection based on dual-frequency C/N0 data," GPS Solutions, Vol. 23, No. 1, 2019, pp. 1-13.
doi: 10.1007/s10291-018-0799-6.
[14] Xu B, Jia Q, Luo Y, Hsu LT, "Intelligent GPS L1 LOS/multipath/NLOS classifiers based on correlator-, RINEX- and NMEA-level measurements," *Remote Sensing*, Vol. 11, No. 16, 2019.
doi: 10.3390/rs11161851.
[15] Hegarty C, Tran M, Corporation TM, Dierendonck AJ Van, Systems AJ, "Acquisition Algorithms for the GPS L5 Signal," *ION GPS/GNSS*, No. September, 2003, pp. 9-12.
[16] Kaplan E Hegarty C, Understanding GPS/GNSS: Principles and Applications, Third. Artech, 2017.
[17] Leclère J, Botteron C, Farine PA, "Acquisition of modern GNSS signals using a modified parallel code-phase search architecture," *Signal Processing*, Vol. 95, 2014, pp. 177-191.
doi: 10.1016/j.sigpro.2013.08.004.
[18] Arul Elango G, Sudha GF, Francis B, "Weak signal acquisition enhancement in software GPS receivers – Pre-filtering combined post-correlation detection approach," *Applied Computing and Informatics*, Vol. 13, No. 1, 2017, pp. 66-78.
doi: 10.1016/j.aci.2014.10.002.
[19] Leclère J, Landry R, Botteron C, "Comparison of L1 and L5 Bands GNSS signals acquisition," *Sensors (Switzerland)*, Vol. 18, No. 9, 2018.
doi: 10.3390/s18092779.
[20] Krumvieda K, et al., "A complete IF software GPS receiver: A tutorial about the details," Proceedings of the 14th International Technical Meeting of the Satellite Division of The Institute of Navigation (ION GPS 2001), No. January, 2001, pp. 789-829, [Online]. Available:
http://www.ion.org/search/view_abstract.cfm?jp=p&idno=1757
[21] Ward, PW, "GPS Receiver Search Techniques," IEEE, 1996.
[22] Franceschetti M, Wave Theory of Information, First. Cambridge University Press, 2017.
doi: 10.1017/9781139136334.